A Wear Model for Silicon Nitride in Dry Sliding Contact against a Nickel-Base Alloy

Iyas Khader[1,2] *, Alexander Renz[2,3], Andreas Kailer[2]

[1] Department of Industrial Engineering, German-Jordanian University, P.O. Box 35247, 11180 Amman, Jordan

[2] Fraunhofer Institute for Mechanics of Materials IWM, Wöhlerstraße 11, 79108 Freiburg, Germany

[3] Luleå University of Technology, 971 87 Luleå, Sweden

*Corresponding author: iyas.khader@gju.edu.jo

Abstract

The properties of silicon nitride ceramics allow their broad application in extreme tribological conditions. High-temperature sliding contact of Si_3N_4-base materials against metals will be found more often in future applications, in which the ceramic's wear resistance becomes clearly necessary.

In this study, the dry sliding behavior of silicon nitride against Inconel 718 is investigated. Wear experiments were carried out at sliding velocities ranging from 1 to 20 m/s. A finite element wear simulation was constructed by relying on experimentally measured wear rates and COF. The simulations enabled quantifying localized temperature and contact stress fields as a function of geometrical changes due to progressive wear.

The experiments showed a transition in wear mechanisms depending on the sliding velocity and frictional power. Cross-sectional analysis of the ceramic samples provided information on the tribochemical processes and the dominant wear mechanisms. Combining analytical and numerical results enabled proposing a schematic wear model. The agreement of this model with common theories of wear is discussed.

Keywords: *silicon nitride; nickel-base alloy; tribochemical wear; modeling wear*

1 Introduction

The application of engineering ceramics in machining high strength alloys such as nickel-base superalloys is widely used. While the effect of mechanical load on the sharp edges of the tool may be mitigated through proper tool design and usage, tribological load by sliding remains as an origin of wear and can be considered as the crucial factor in limiting the lifetime of the tool. In an early review of the application of engineering ceramic tools in machining Stachowiak and Stachowiak [1] explained tool wear to originate from mechanically activated mechanisms by abrasion and adhesion, and tribochemical wear driven by chemical interaction between the tool, workpiece, and surrounding media at high contact surface temperatures. These tribochemical interactions are activated at high contact surface temperatures, depending on the energy dissipation and hence on the sliding speeds, as well as on the chemical affinity of the materials to each other [2]. A recent review on tool wear mechanisms in general can be found in Olortegui-Yume and Kwon [3] and specifically in machining nickel-base alloys in Zhu et al. [4]. A review on the influence of tool materials on the machinability of nickel-base alloys is given by Pervaiz et al. [5]. Whereas, the synergetic and/or competing mechanical and chemical wear mechanisms involved in ceramic cutting tools were addressed by [6, 7].

The mechanical and physical properties of silicon nitride indicate good resistance to thermal shock. Nevertheless, previous research work has indicated chemical instability of silicon nitride ceramics in some systems such as in contact with molten copper in the presence of oxygen [8] and molten steel [9], and in sliding contact against ferrous alloys [10]. It also showed susceptibility to tribochemical wear in machining steel [11], especially chromium containing steel alloys [12], whereas, in machining Inconel 718 nano-grained silicon nitride showed high wear rates due to nose wear according to [13]. Diffusion tests in vacuum were conducted by Addhoum and Broussaud [14] using SiAlON (an Si_3N_4-base ceramic with additional content of aluminum and oxygen) against Inconel 718 and Waspaloy static interaction couples. The authors described the formation of a liquid phase corrosion layer at temperatures exceeding 1100 °C with precipitation of TiN at its interface in the metal side and the presence of nickel, iron, and chromium silicides in the corrosion layer. On the

other hand, Si_3N_4 was mentioned in [15] to have a rather high resistance to interaction with nickel even in its molten state. Renz [16] conducted diffusion tests in air on SiAlON against Inconel 718 and Nimonic 90 static interaction couples and reported the formation of chromium and titanium oxides at high temperatures. Bhattacharyya et al. [17] tested commercial SiAlON inserts by machining Incoloy 901 and found wear by attrition and diffusion to control the tool life up to certain cutting speed.

In order to obtain accurate information on the tribological behavior of any material combination in contact, tribological experiments under controlled environments have to be designed and conducted. Supporting the experiments, numerical modeling offers the possibility of estimating quantitative data such as contact surface temperatures and localized stress fields, both of which are almost impossible to measure in situ. In a recent study by Renz et al. [18] the dry sliding behavior of two cutting tool materials, namely, a SiAlON and a silicon carbide (SiC) whisker reinforced alumina (Al_2O_3) composite, against Inconel 718 was studied in detail. The authors pinpointed a combination of mechanically activated and tribochemical wear mechanisms involved in the wear of the ceramic samples tested in dry sliding contact experiments.

The current study focuses on the wear behavior of a gas-pressure sintered silicon nitride in dry sliding against Inconel 718. Gas-pressure sintered silicon nitride is lately gaining much more importance in engineering applications, especially in cutting and forming tools and dies, due to its less expensive yet more versatile manufacturing technique as opposed to its hot-pressed counterpart. The high cost incurred by the fabrication of hot-pressed silicon nitride in addition to the intrinsic limitations imposed by the process in producing parts with complex geometries both have kept its application limited. Moreover, studying a simple silicon nitride ceramic provides fundamental knowledge needed in developing tailored Si_3N_4-base material systems for various applications. This work combines experimental work and finite element simulations, by which the ceramic-metal contact was modeled to obtain information on localized temperature and contact pressure fields as functions of progressive wear. Macroscopic wear was implemented within the finite element framework in the

commercial software ABAQUS by modeling smooth surfaces in contact and through a bespoke subroutine to account for wear. The effect of wear on the contact conditions is correlated with the experimental outcomes, thus, enables a better understanding of the wear mechanisms, and friction behavior observed in the experiments.

2 Experimental

A commercially available Si_3N_4-base ceramic (SN-GP black, FCT Ingenieurkeramik GmbH, Germany) was tested in unlubricated sliding contact experiments against Inconel 718 (EN material no. 2.4668) disks (initial average surface roughness R_a=1.06±0.13 µm), Fig. 1a. The ceramic samples were provided by the manufacturer in a CNGN-type insert geometry, Fig. 1b. The tests were run in the configuration shown in Fig. 1c.

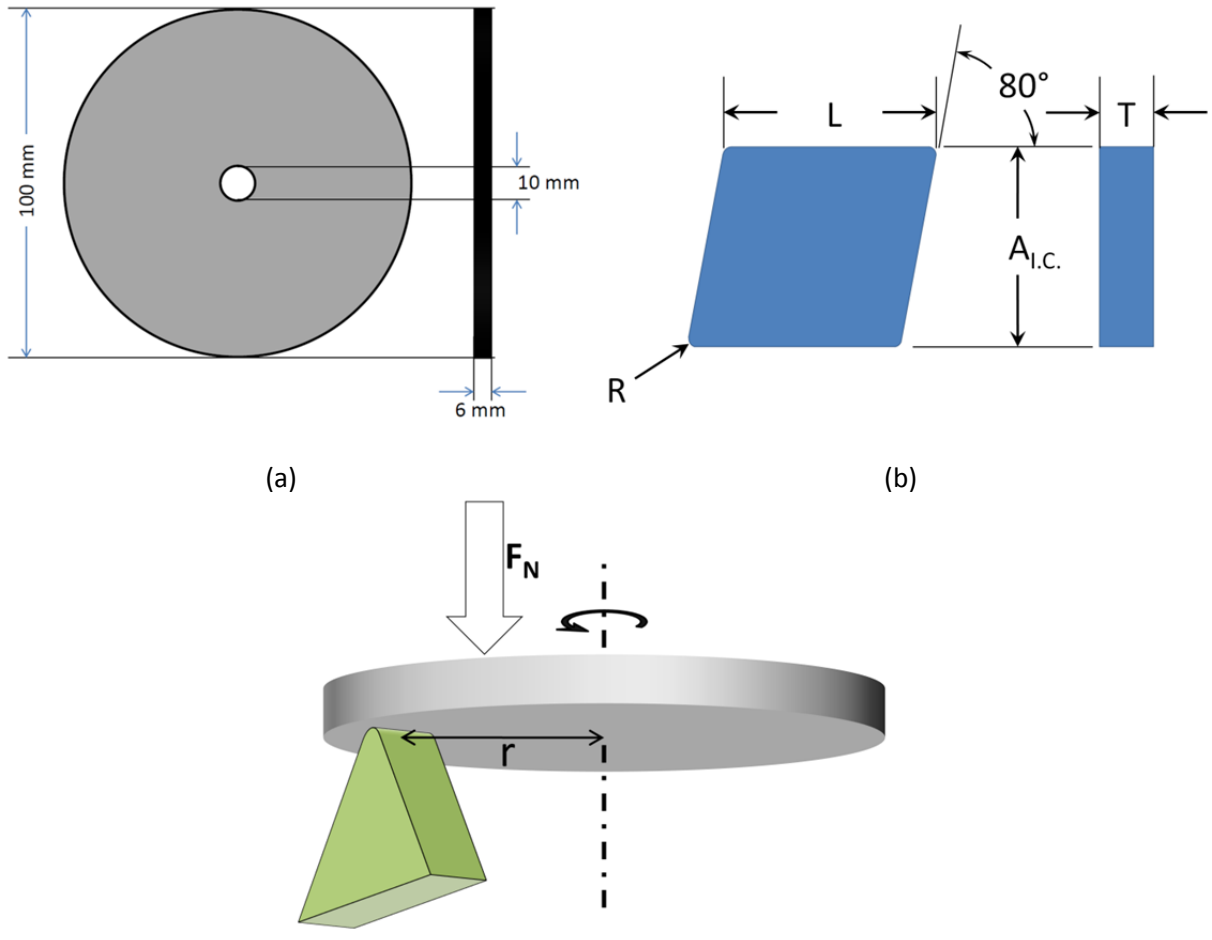

Fig. 1. Schematic drawings of (a) the Inconel 718 disk, (b) the SN-GP black ceramic samples (L = 12.9 mm; $A_{I.C.}$ = 12.7 mm; T = 3.0 mm, and R = 0.8 mm), and (c) the pin-on-disk test configuration

SN GP black is a commercial Si_3N_4-Y_2O_3-Al_2O_3 material system. Its microstructure consists of β-Si_3N_4 grains and ca. 10 wt.% secondary glassy phase of the sintering additives and less than 1 wt.% Ti. The β-Si_3N_4 grains have a length-to-diameter ratio of L/D=7.4. The microstructure of SN-GP black is shown in a backscattered mode scanning electron microscope (SEM) image in Fig. 2. The temperature dependent properties of SN-GP black were obtained from a series of experiments aimed at characterizing the material in [19]. The chemical composition of Inconel 718 is listed in Table 1.

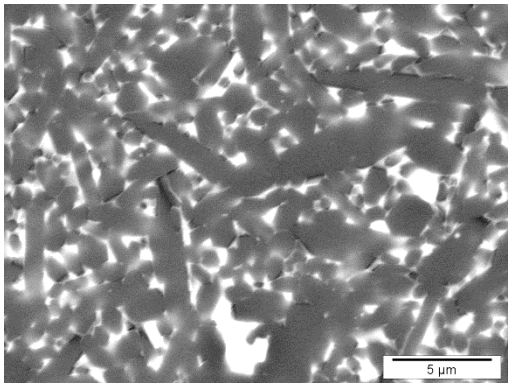

Fig. 2 Backscattered SEM image of the microstructure of SN-GP black

Table 1. Limiting chemical composition of Inconel 718 as provided by the manufacturer [20]; elements of concentrations below 0.4 at.% are not listed; melting point T_m=1336 °C; shaded elements are present in the chemical composition of SN-GP black

Element	Ni+Co	Cr	Fe	Nb+Ta	Mo	Co	Mn	Ti	Si	Al	N	O	Y
At.%	50-55	17-21	*	4.8-5.5	2.8-3.3	1.0	0.4	0.7-1.2	0.4	0.2-0.8	-	-	-

* balance

The side faces of the ceramic samples were ground. The samples were then fixed into a tribometer using a special fixture designed to withstand the tangential forces emerging in dry sliding contact. A 3 mm line contact is created between the edge of the insert-like ceramic sample (R=0.8 mm, see schematics in Fig. 1b) and the flat surface of the Inconel 718 disk. From the Hertzian contact theory the resulting semi contact width at an applied normal force of 100 N is approximately 20 µm, corresponding to an initial contact pressure of ca. 1.4 GPa. The experimental parameters are listed in Table 2.

Table 2. Experimental parameters of the unlubricated sliding-contact experiments

Materials	SN-GP black/Inconel 718
Applied normal load [N]	100
Sliding velocity of the ceramic samples [m/s]	1, 2.5, 5, 7.5, 10, 15, 20 (at the center of contact)
Sliding distance [m]	2000
Lubricant	no lubrication (dry sliding)
Atmosphere	air
Temperature	room temperature (held constant at 24 °C)

Scanning electron microscopy (SEM) and energy-dispersive X-ray spectroscopy (EDX) were carried out on the contact surfaces and polished cross sections prepared from the ceramic samples. Progressive wear throughout the tests changes the contact geometry from line to flat-like contact and accordingly the contact area increases. Fig. 3. shows the geometry of a sample demonstrating the wear volume. The worn volume of in the ceramic samples was obtained by measuring the linear wear (V_T) and the width of specimen wear land (V_B) and taking into account the profile of the sample. The dependence of contact area, contact pressure, and wear depth is shown in Fig. 4. Wear rates of the ceramic samples were calculated from the volume loss using microscopic measurements of the geometrical changes.

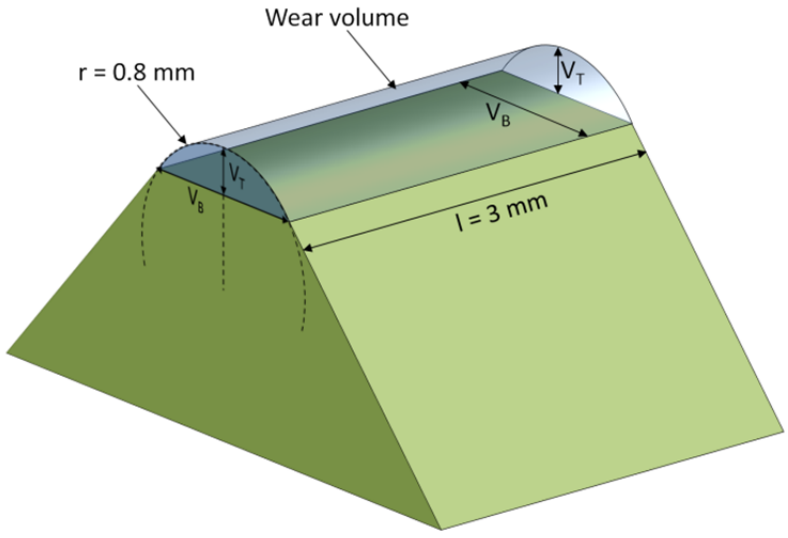

Fig. 3. Schematic illustration of the worn volume in the ceramic sample due to sliding contact

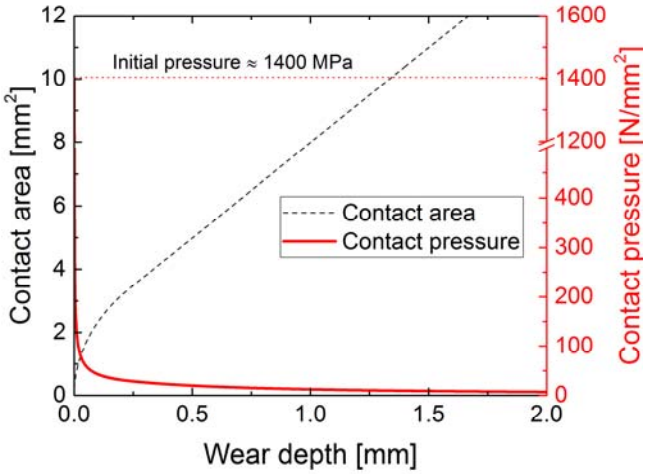

Fig. 4. Change of contact area (dashed line) and contact pressure (solid line) as functions of progressive wear

In order to better understand the observed wear behavior in dry sliding, a correlation was established between the macroscopic wear coefficient *K*, given by

$$K = \frac{V_w}{F_N s} \tag{1}$$

and the frictional power P_f;

$$P_f = F_f \dot{s} = \mu F_N \dot{s} \tag{2}$$

where V_w is the wear volume in ceramic, s is the sliding distance, F_N is the applied normal force, F_f is the friction force, μ is the coefficient of friction (COF) and $\dot{s}$ is the sliding velocity; the sliding distance was set to 2000 m for all tests. Plotting the wear coefficient *K* against the frictional power takes the changing COF into account and thus provides a more generalized view of the tribological system.

3 Numerical simulations

Finite element simulations were used to model dry sliding. The aims of the modeling are twofold: to obtain approximate localized contact surface temperatures, and to understand the effect of wear and geometrical changes on the nature of contact.

Sliding contact was modeled using a coupled thermal-mechanical two-dimensional plane-stress finite element simulation in ABAQUS/Standard. The line contact occurring between the ceramic and metal samples renders the problem ideal for two-dimensional modeling, see Fig. 5.

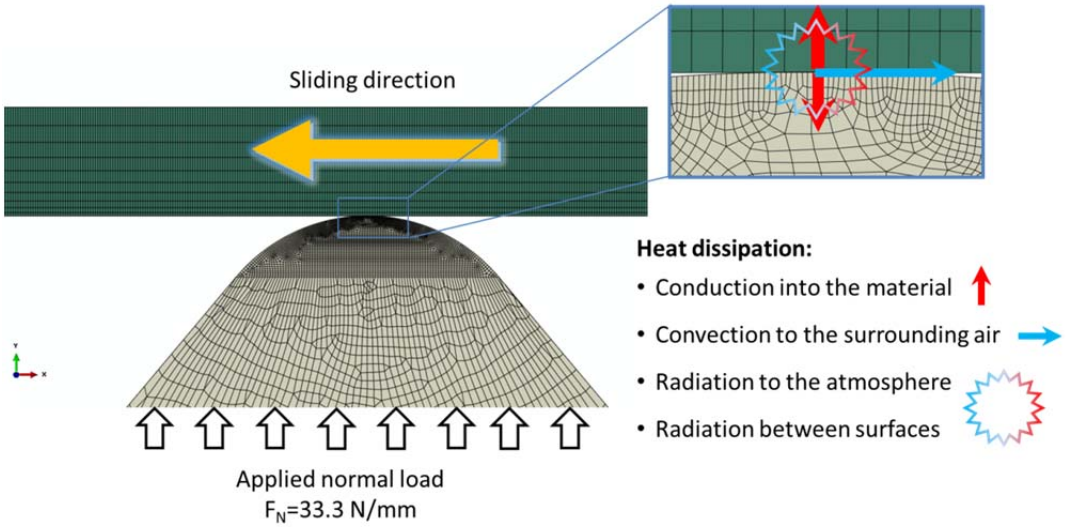

Fig. 5 Illustration of the contact configuration in two dimensions showing the FE mesh

The model was comprised of the tip of the ceramic sample having a radius of 0.8 mm and a contact length of 3 mm, upon which a normal load of F_N=100 N was evenly distributed. The metallic disk was modeled as a rotating ring to take into account the heat build-up on its surface. Once the contact was initialized between the two bodies, the disk was rotated at a prescribed rotational velocity. Coulomb friction was assumed between the surfaces in contact with a constant COF obtained experimentally (refer to Section 4). The COF was set to $\mu = 0.54$ and $\mu = 0.14$ for sliding velocities of 1 m/s and 20 m/s, respectively.

Four-node first-order plane-stress elements with displacement and temperature degrees of freedom (CPS4T) were used to discretize the geometry.

The mechanical behavior of SN-GP black was obtained from a series of experiments aimed at characterizing the material [19]. The elastic modulus and thermophysical quantities of SN-GP black are shown in Fig. 6.

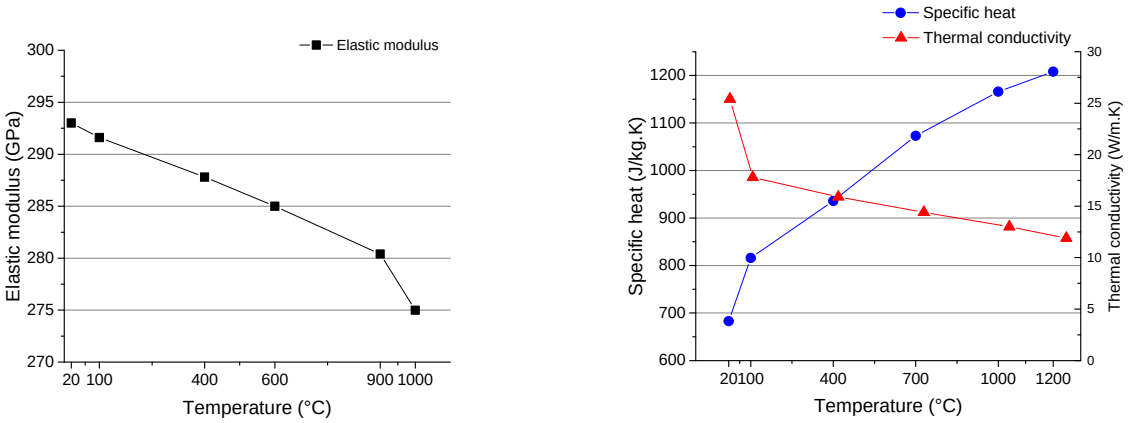

(a) (b)

Fig. 6. Temperature dependent properties of SN-GP black (a) elastic modulus, (b) specific heat and thermal conductivity

Average values for Poisson's ratio and the thermal expansion coefficient of SN-GP black over the temperature range 20-1000 °C were experimentally measured in [19] and found to be 0.26 and 3.5×10^{-6} K^{-1}, respectively.

The mechanical behavior and thermophysical properties of Inconel 718 were obtained from [20]. For simplicity, a strain rate independent elastic-plastic mechanical model was adopted to account for plastic deformation in Inconel 718; any phase transformation occurring in the alloy was neglected.

3.1 Calculation of the contact surface temperature

In order to resolve temperature fields with high accuracy within the contact zone, a dense mesh was created in the vicinity of the contacting surfaces. The average element size in the contact zone was 16 µm in the horizontal direction and 10 µm in the vertical direction.

The implemented heat transfer model taken into account: (i) frictional heat generation, (ii) heat conduction between the contacting bodies, (iii) natural convection to the surrounding air, (iv) radiation to the atmosphere, and (v) radiation between both surfaces. A transient solver was adopted for the heat transfer problem.

The frictional heat generation was calculated from the frictional stress and slip rate, by which the overall specific frictional energy dissipation rate (i.e., frictional power) is given by

$$P_f = \tau \dot{s} \qquad (3)$$

where τ is the frictional stress and $\dot{s}$ is the slip rate (i.e., sliding velocity). The heat flux passing into each surface is given by

$$q_1 = f\eta P_f \quad (4)$$

$$q_2 = (1-f)\eta P_f \quad (5)$$

where f is the weighting factor for distribution of the heat between the interacting surfaces and η specifies the fraction of dissipated energy converted into heat where $0 \leq \eta \leq 1.0$.

From experimental observations, it is obvious that the contact conditions and the interface properties change during sliding (see Fig. 4). The distribution of heat between the sliding surfaces depends on the difference in thermo-physical properties of the contacting materials among several other factors including the temperature difference, sliding speed, and duration of contact (cf. Barber [21] and Komanduri and Hou [22]) in addition to the interface properties such as the formation of oxides (e.g., Quinn [23]). Here, it was assumed that both surfaces receive an identical amount of heat (i.e., $f = 0.5$), since obtaining validated experimental results for these values is very difficult.

It is not known a priori what fraction of the overall frictional energy is converted into heat. By relying on an energy based approach (see Fleischer [24] and Fleischer [25]), it can be assumed that the total energy dissipation is shared by three parts, namely, heat, generation of wear, and change of materials [26]. The strain energy density of fracture for SN-GP black (measured fracture toughness: K_{IC}=5.62±0.09 MPa·m$^{1/2}$ [19]) would comprise a small amount of the dissipated energy which should not exceed 10%. Hence, for the case $\dot{s}$ =1 m/s (where mechanical wear is dominant as portrayed in Section 4.1) the fraction of energy dissipated as heat was set to η =0.9. At higher sliding velocities, energy dissipation in tribochemical reactions (see Section 4.1) has its considerable share of the overall frictional energy. A rough calculation may be achieved by considering the enthalpy change of formation of reaction products [27], thus, leading to a value of η =0.4 for the set of simulations run at $\dot{s}$ =20 m/s.

Conduction heat transfer was taken into account by modelling thermal resistance between the two surfaces in contact; the interface conductance was assumed to be pressure dependent with values in the range between h_{ic}=1500 W/m^2.K and h_{ic}=8500 W/m^2.K [28]. The convection heat transfer to the surrounding air was accounted for by calculating an approximate natural convection heat transfer coefficient ($\bar{h}_{nc}$=15 W/m^2.K) at a sink temperature of T_{SC}=20 °C. Radiation was incorporated into the thermal model by assuming a sink temperature of T_{SR}=293.15 K. Emissivity values of 0.9 and 0.5 were adopted for silicon nitride [29, 30] and Inconel 718 [31], respectively.

3.2 Modeling wear

In order to incorporate macroscopic wear in the simulation, the user subroutine UMESHMOTION was used. This subroutine acquires material and position data from the FE model and returns incremental nodal sweeps in the local normal direction to be applied as adaptive mesh constrains on surface nodes. The incremental nodal sweeps are dependent on the value of the incremental wear computed within the UMESHMOTION algorithm [32].

The volumetric wear rate for the whole contact area was calculated by relying on an adapted form of the Holm-Archard [33, 34] wear equation,

$$\dot{V}_w = KpA\dot{s} \tag{6}$$

where $\dot{V}_w$ is the volumetric wear rate, K is the wear coefficient given in Eq. (1) and experimentally obtained from the tribological tests, p is the contact pressure within the contact area A and $\dot{s}$ is the slip rate. To implement Eq. (6) in a finite element form and calculate the incremental volumetric wear, the rate of nodal ablation is expressed by

$$\frac{dh}{ds} = Kp \tag{7}$$

where dh is the incremental change in height, and ds is the incremental nodal slip, and thus the computation of wear is based on the local contact pressure p. It is worth noticing that the contact pressure in Eq.(6) and (7) in addition to being a function of the applied normal load and the geometry

of the surfaces in contact, is an implicit function of temperature manifested by temperature dependent material properties adopted in the FE models.

To simplify the simulations and since geometrical changes in the metallic disk during sliding will not affect the contact configuration, wear was only implemented in the ceramic tip. Moreover, and due to the complexity of the model, only a finite number of rotations can be simulated, thus, a siding distance of 1000 mm was considered.

4 Results

4.1 Experimental results

The coefficient of friction μ was obtained from the measured torque during the tests. The COF as function of sliding distance for different sliding velocities is shown for some tests in Fig. 7. Two observations can be made: with increasing sliding velocity the value of μ decreases and the scatter about its mean value becomes smaller.

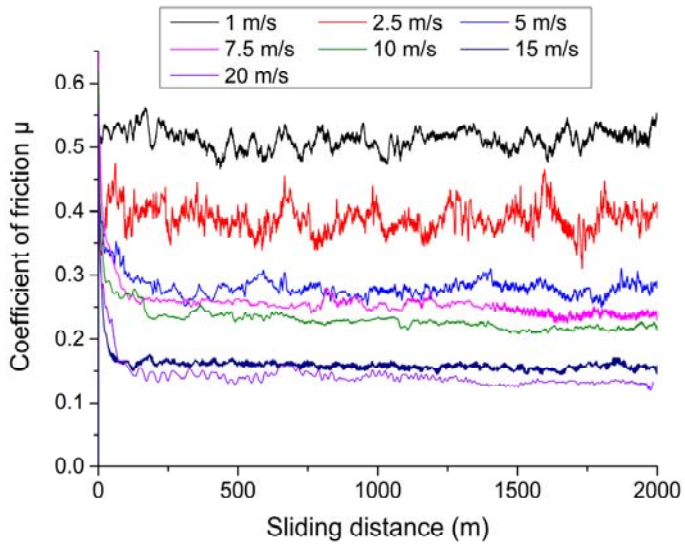

Fig. 7. Coefficient of friction for SN-GP black in dry sliding against Inconel 718 for different sliding velocities at a normal force of F_N=100 N

The measured wear volume from the ceramic samples and the corresponding COF are plotted against the sliding velocity in Fig. 8.

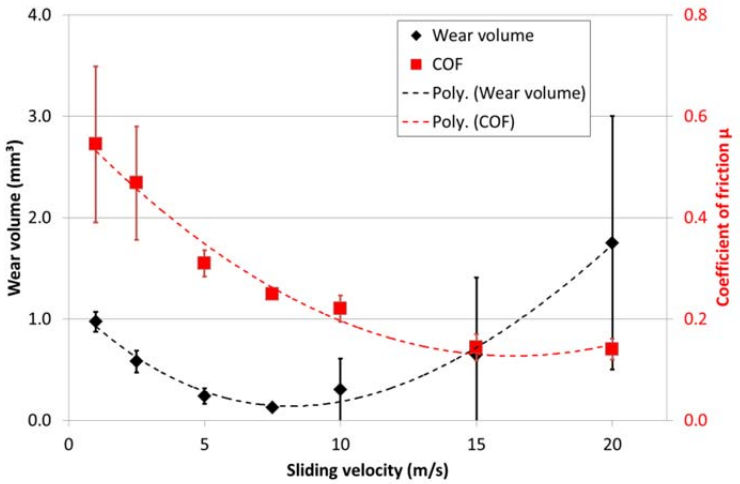

Fig. 8: Wear volume and coefficient of friction (mean values) plotted against the sliding velocity; dashed lines: 2nd order polynomial for the wear volume, 3rd order polynomial for the COF

The COF and wear volume data were used to calculate the wear coefficient *K*, refer to Eq. (1); the results are plotted in Fig. 9 against the frictional power calculated in Eq. (2).

The wear coefficients adopted in the simulations, Eq. (7), were $K = 4.86\times10^{-6}$ mm^3/N·m and $K = 8.75\times10^{-6}$ mm^3/N·for sliding velocities of 1 m/s and 20 m/s, respectively.

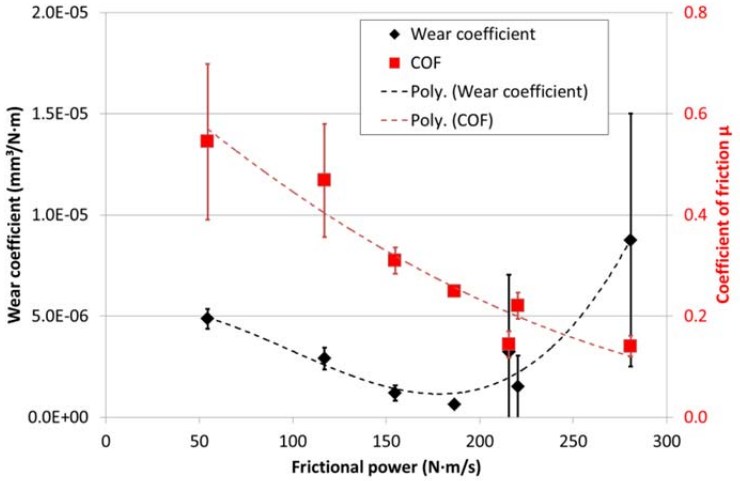

Fig. 9: Wear coefficient, Eq. (1), and coefficient of friction (mean values) plotted against the frictional power; dashed lines: 2nd order polynomial for the wear volume, 3rd order polynomial for the COF

The wear volume in Fig. 8 shows decreasing wear rates up to a sliding velocity of ca. 7.5 m/s, at which point a minimum is reached. Further increase in sliding velocity increases the wear rate. The same trend is observed for the wear coefficient plotted against the frictional power in Fig. 9. Therefore, detailed microscopic analysis of selected worn ceramic samples tested at 1.0, 5.0, and 20 m/s were conducted. At a sliding velocity of 1 m/s (Fig. 10a) mechanical wear of silicon nitride is visible in addition to a built-up metallic transfer layer. β-Si_3N_4 grains are dislodged from the ceramic

surface and some are embedded within the metallic transfer layer; fatigue of the ceramic microstructure can be observed. At 5 m/s (Fig. 10b) the detached β-Si_3N_4 grains embedded in the metallic layer appear smaller and in lighter contrast in comparison to the intact grains appearing in the same SEM image, thus, indicating chemical modification to their original composition. Cross sectional analysis on samples tested at 20 m/s (Fig. 10c) reveal a ca. 10 µm wide layer separating the ceramic from the metallic build-up (referred to as "tribochemical layer" in Fig. 10c); a smaller less pronounced intermediate zone appears just at the interface between the ceramic and this aforementioned "tribochemical layer". A more detailed compositional analysis is shown in Fig. 11.

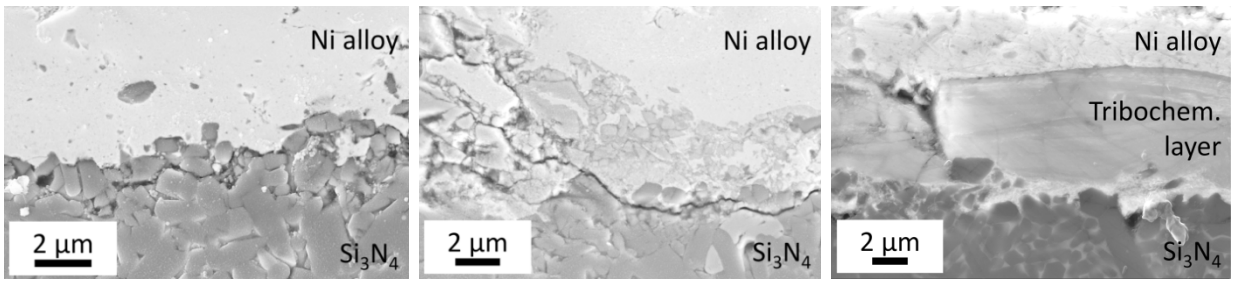

(a) (b) (c)

Fig. 10: SEM images of polished cross sections of ceramic samples tested at a sliding velocities of (a) 1 m/s, (b) 5 m/s, and (c) 20 m/s

High magnification SEM and elemental analysis conducted on samples tested at 20 m/s indicated the presence of four distinct zones labeled in Fig. 11 as follows: zone (1) silicon nitride, zone (2) an intermediate zone, zone (3) a reaction tribolayer, and zone (4) a transfer metallic layer from the Inconel 718 alloy. Zone (3) shows high concentrations of O, Cr, Al, and Ti, and low to very low concentrations of Nb, Co, Si, Mo, Fe, and Y (Co, Mo, and Y are not shown in the linescan in Fig. 11). No traces of N were detected in this zone.

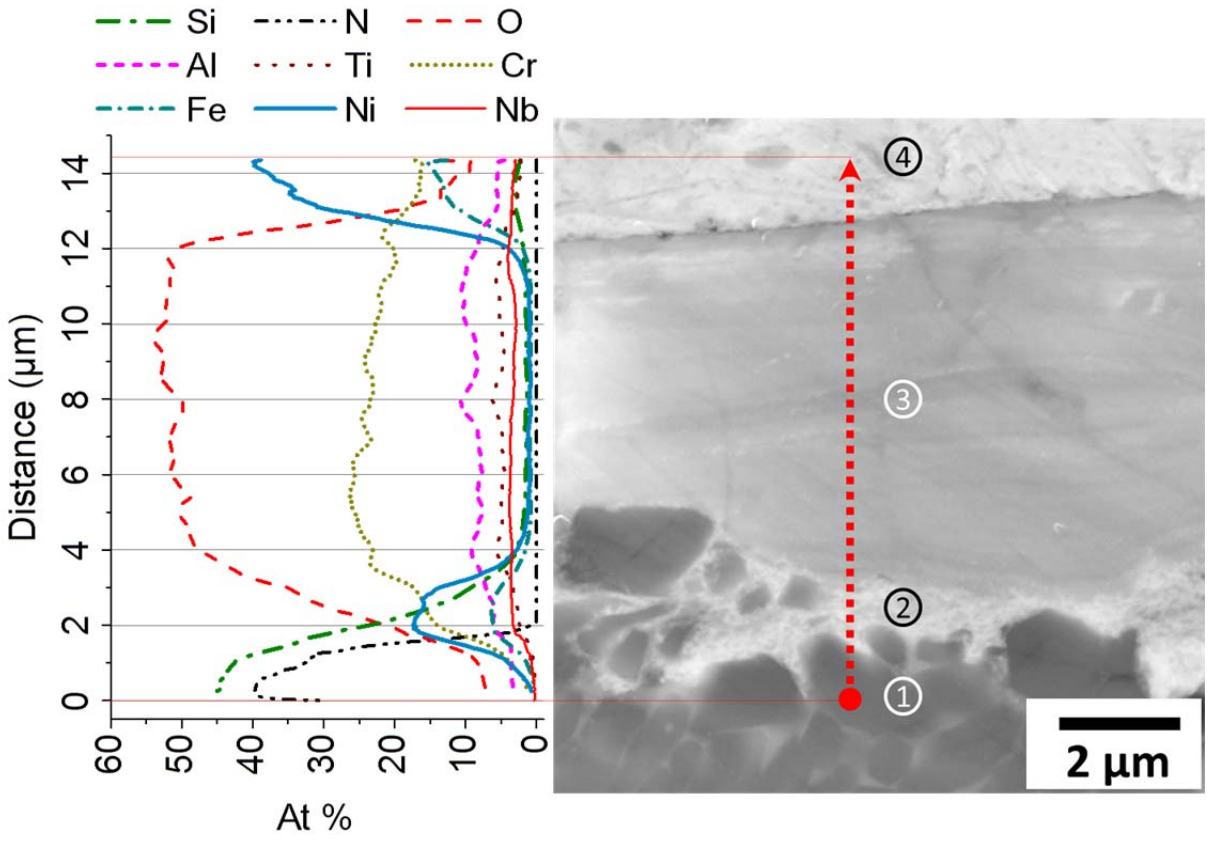

Fig. 11: (right) SEM image of a polished cross section of a ceramic sample tested at a sliding velocities of 20 m/s, (left) EDX linescan along a line passing through four discernable zones (only significant elements are shown)

Zone (2), which can be described as an intermediate layer between the ceramic and the reaction tribolayer, contains high concentrations of Ni and Fe. The EDX linescan shows positive concentration gradients of O, Cr, Al, Ti, and Nb in zone (2) towards zone (3) and negative gradients of Si in zone (2) towards zone (3). The concentration of N decreases sharply at the interface between zone (1) and zone (2) and reaches zero after fractions of a micrometer within zone (2).

Samples of wear debris from tests carried out at various sliding velocities, namely, 1, 5, 7.5, and 20 m/s were investigated as shown in Fig. 12.

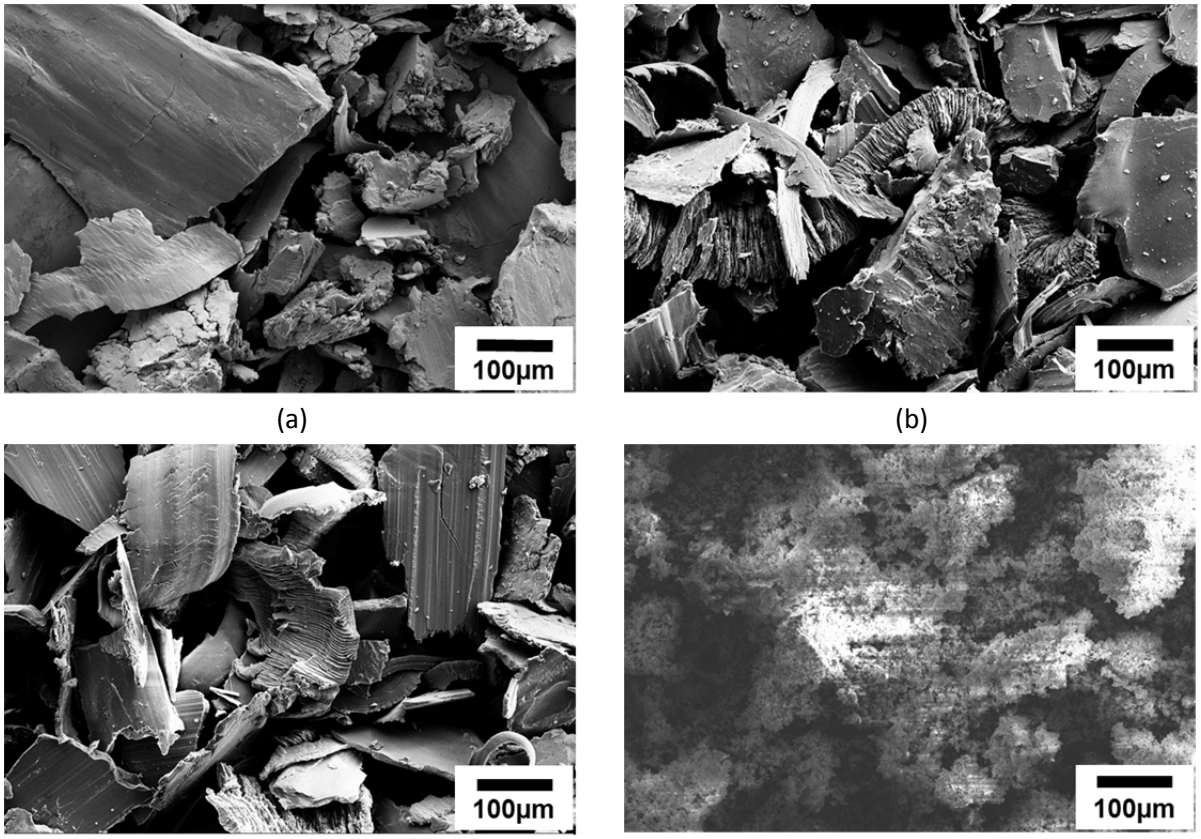

(a) (b)

(c) (d)

Fig. 12 SEM images of wear particles generated at a sliding velocities of (a) 1m/s, (b) 5 m/s, (c) 7.5 m/s, and (c) 20 m/s

A summary of the EDX analysis of the wear particles is shown in Fig. 13.

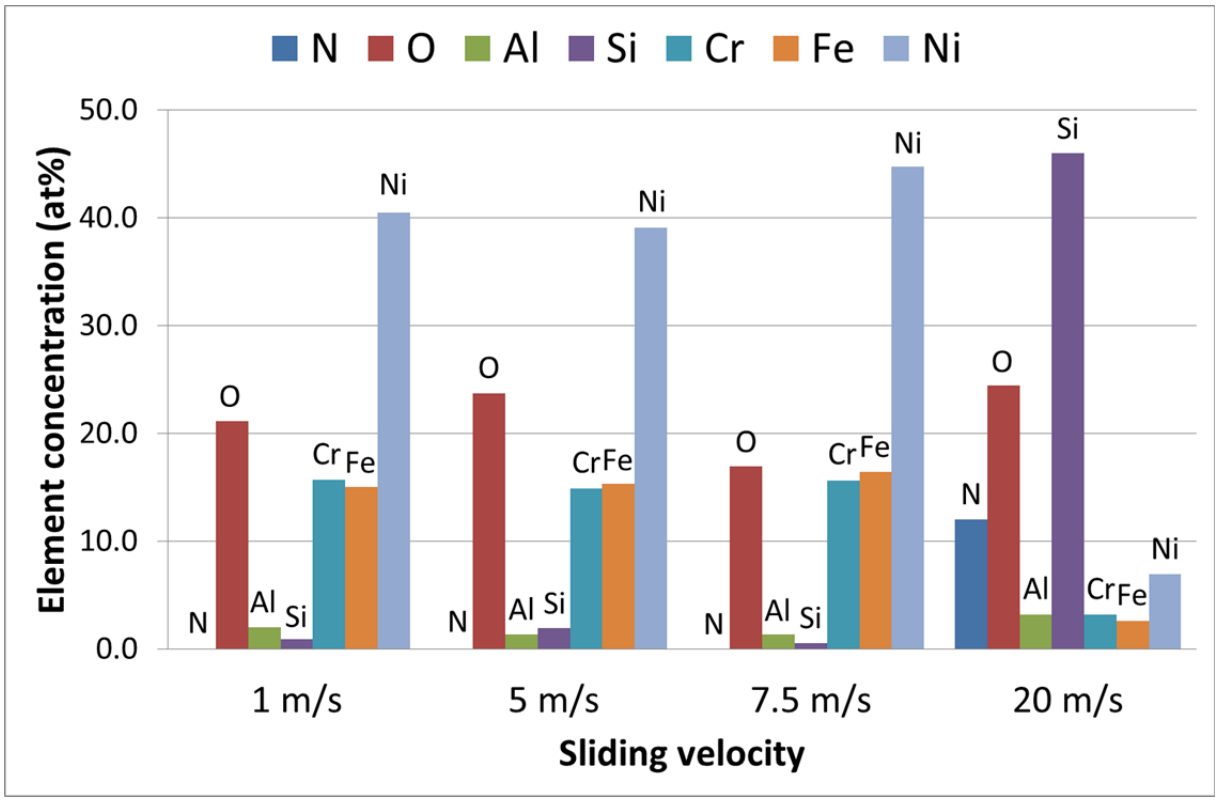

Fig. 13: Comparison of wear particle composition (relevant elements only)

The wear debris generated from samples tested at 1 to 7.5 m/s is mainly composed of plastically deformed chip-like metallic particles from the nickel-base alloy. Little change is observed by increasing the sliding velocity from 1 to 7.5 m/s. The cracks and rough edges indicate limited plastic deformation, whereas the presence of abrasion grooves points out towards abrasion dominated wear in the nickel-base alloy. At 20 m/s the wear debris appears as fine grained porous structure that is electrically non-conductive as suggested by the bright electrically charged areas in the SEM image in Fig. 12d.

For sliding speeds up to 7.5 m/s, the wear debris is mainly composed of oxides of the nickel-base alloy elements as shown in the EDX results, Fig. 13. On the other hand, the wear debris collected from tests carried out at 20 m/s reveals increased concentrations of Si, N, and Al, which are the major constituents of the ceramic, whereas, elements of the nickel-base alloy are present in relatively smaller concentrations. The high concentration of O still indicates that and oxidation reaction took place.

4.2 Numerical results

The results of the FE simulations were obtained for a sliding distance of 1000 mm and sliding velocities of 1 m/s and 20 m/s. By adopting the experimentally obtained tribological parameters (for 1 m/s: $K = 4.86\times10^{-6}$ mm^3/N·m and $\mu = 0.54$, and for 20 m/s: $K = 8.75\times10^{-6}$ mm^3/N·m and $\mu = 0.14$), the ablation in height for the two sliding velocities is shown in Fig. 14.

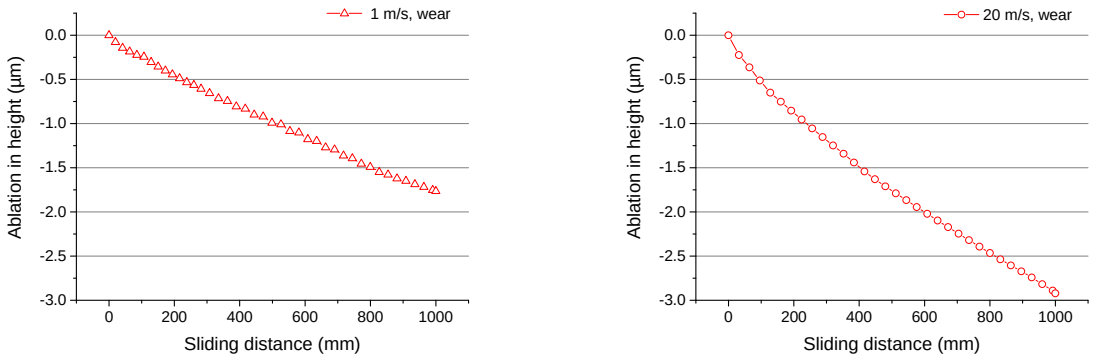

(a) (b)

Fig. 14. FE generated plot for the ablation in height against sliding distance for (a) 1 m/s, (b) 20 m/s

A comparison between the contact surface temperature as a function of sliding distance obtained by considering the initial contact geometry (unworn configuration) and by implementing progressive wear is shown for both sliding velocities in Fig. 15.

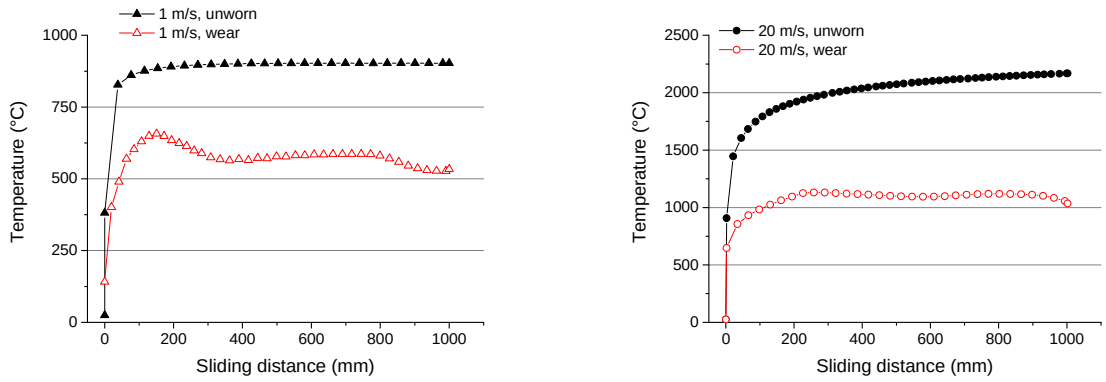

(a) (b)

Fig. 15. FE generated contact surface temperature in ceramic against sliding distance for (a) 1 m/s, (b) 20 m/s

The temperature contour plots for both unworn and worn configurations are shown for both sliding velocities in Fig. 16. At 1 m/s, the maximum temperature reaches 902.7 °C and 534.1 °C in the unworn and worn configurations, respectively. The radius of the zone with a temperature exceeding 534.1 °C in the unworn configuration is ca. 25 µm (region marked in gray in Fig. 16a). At 20 m/s, the maximum temperature reaches 2168.6 °C and 1042.5 °C in the unworn and worn configurations, respectively. The radius of the zone with a temperature exceeding 1042.5 °C in the unworn configuration is ca. 33 µm (region marked in gray in Fig. 16c). The corresponding maximum contact surface temperature of the Inconel 718 disk (T_{disk}) is shown in Fig. 16.

The contact pressure is considerably affected by the implementation of wear and the consequent change in contact area. A comparison between the contact pressure as a function of sliding distance for the unworn geometry and that obtained with implemented wear is shown for both sliding velocities in Fig. 17.

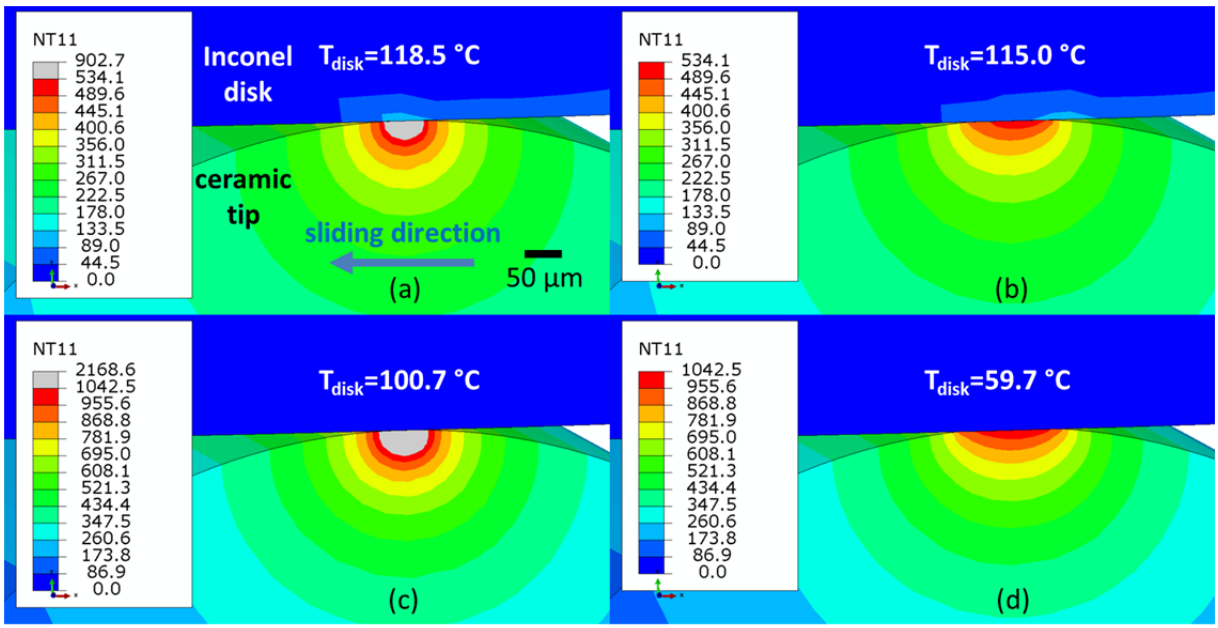

Fig. 16: FE generated contours of nodal temperature at the contact zone (a) 1 m/s unworn configuration, contact patch width $b = 33.5$ µm, (b) 1 m/s worn tip, $b = 100.5$ µm, (c) 20 m/s unworn configuration, $b = 33.9$ µm, and (d) 20 m/s worn tip, $b = 134.8$ µm; s=1000 mm; T_{disk} is the maximum contact surface temperature on the disk

(a) (b)

Fig. 17. FE generated plots for the contact pressure against sliding distance for (a) 1 m/s, (b) 20 m/s

5 Discussion

An energy threshold, i.e., activation energy, has to be overcome to initiate any form of chemical reaction. In the case of tribochemical wear, the energy barrier needed to trigger such reactions may be described as a function of both thermal energy and mechanical stresses (cf. Jacobs et al. [35] Jacobs and Carpick [36] and Gosvami et al. [37]). The simulations showed the influence of sliding velocity on the contact surface temperature, which has a direct effect on the tribological behavior of the mating pairs. This theoretical correlation explains the quantitative wear behavior observed in Fig.

8 as a function of sliding velocity and in Fig. 9 as a function of frictional power. At low sliding velocities, wear is mostly dominated by attrition (adhesive wear) as observed in Fig. 10a, in which individual β-Si_3N_4 grains appear to be detached from the ceramic structure and become embedded into the metallic transfer layer. The contact surface temperature at this sliding velocity is not high enough to trigger high rates of diffusion, which usually follow an Arrhenius-type equation. Nevertheless, one cannot exclude the effect of cyclic fatigue and microcracking on the generation of wear debris. The lowest wear volume and wear coefficient are observed at a sliding velocity of 7.5 m/s, which corresponds to a frictional power of 180 N·m/s.

Microstructural analysis provided more details on the prevailing wear mechanisms. The SEM cross-sectional analysis confirms changes in the morphology of the formed tribolayers with increasing sliding velocity. Fig. 10b shows the formation of a heterogeneous phase (it sometimes appears in the form of discrete patches) at the interface between silicon nitride and the metallic transfer layer and signs of chemical and mechanical degradation of the detached β-Si_3N_4 grains. At this point, it can be argued that the prevailing localized contact conditions, i.e., temperature and stress, have reached a level that accelerates chemical reactions. Similar results were obtained by Brandt et al. [38] by carrying out turning tests at cutting speeds ranging from 150 to 450 m/min (2.5 to 7.5 m/s) and describing the dominant wear mechanism by being mechanical in nature with the presence of chemical reactions.

For the highest sliding velocity, i.e., 20 m/s, high level of wear is observed in Fig. 8, and four discernable zones can be identified in the cross-sectional analysis, Fig. 10c and Fig. 11. In Fig. 11, zone (1) is the intact silicon nitride ceramic and zone (4) is a transfer layer of Inconel 718. Zone (2) may be considered as an intermediate reaction zone originally stemming from the Inconel 718 alloy (in addition to silicon nitride as will be shortly discussed) from which both Cr and Ti are being depleted by diffusion into the tribochemical layer, i.e., zone (3). It is worth noticing that Cr and Ti (and similarly observed for Al and Nb but at much lower concentrations) appear in lower concentrations in zone (2) and in the parent material, i.e., zone (4), than in the tribochemical layer,

zone (3), thus, indicating diffusion of these elements into zone (3). Their positive concentration gradients in zone (2) towards zone (3) support this conclusion. Ni and Fe on the other hand are neither diffusing in the ceramic, zone (1), nor in the tribochemical layer; both elements may be thought of as being trapped in the reaction zone (2) and therefore, appear in high concentrations.

By observing the concentrations of the major constituents of silicon nitride (i.e., Si, N, and O) in zone (2), the EDX analysis reveals positive concentration gradient of O towards zone (3) and considerable, yet declining concentration of Si towards zone (3). Therefore, it can be deduced that, accelerated by high temperatures, silicon oxide may have formed as an intermediate reaction product. The abrupt decrease in nitrogen concentration at the interface between zone (1) and zone (2) supports this assumption as the dissolution of Si_3N_4 into SiO_2 releases N_2 as a gaseous product and hence, it does not appear in the elemental analysis in zone (2).

Corroborating the findings of Bettacharayya et al. [17], the results indicate that chromium, titanium, and to a lower extent niobium are most probably diffusing into the glassy phase of silicon nitride (composed mainly of oxides of silicon, aluminum and yttrium) and weakening its structure by forming metal oxides and thus, promoting wear. On the other hand, the lack of silicon and nitrogen in the tribochemical layer, i.e., zone (3), indicates the unlikelihood of formation of silicides or nitrides [18]. The latter, however, contradicts with the findings of [17] who proposed a diffusion model based on the formation of nitrides instead of oxides in the tribochemical layer.

The COF decreases with increasing sliding velocity, refer to Fig. 8 and Fig. 9. By considering the changes in the tribolayers occurring at different velocities it can be deduced that the tribochemical reactions occurring at high sliding velocity may have a lubricating effect. Such effect is directly in accordance with the conclusions reached by Kramer [2], wherein the author described similar tribochemical wear scenarios to result in reaction products with lower mechanical strength and more susceptibility to wear. Due to their low shear strength, tribochemical layers are easily sheared off, and therefore act as a lubricant, yet, this results in higher wear rates in the ceramic since the newly

formed surface becomes more prone to further reactions. The same behavior was observed in dry sliding of SiAlON against Inconel 718 in [18].

The FEM simulations showed that wear reduces the steady-state contact surface temperature by ca. 40% and 50% for sliding velocities of 1 m/s and 20 m/s, respectively. This comes as a direct consequence of the increased contact surface area and reduction in contact pressure. Here, it should be mentioned that the steady-state value of the COF was adopted in the simulations and hence, conclusions on the influence of the COF during the running-in phase cannot be drawn. From the FE generated temperature contours in Fig. 16, and despite modeling contact as occurring between smooth surfaces, it is still obvious that steep temperature gradients develop in the depth of the ceramic. Such steep gradients make accurate measurements of localized contact surface temperatures, even with high resolution infrared cameras, almost impossible. It is however worth mentioning that Narutaki et al. [39] attempted to measure in situ cutting temperatures in machining Inconel 718 with silicon nitride tools by embedding tungsten wires in the tool before sintering. Moreover, based on the energy method, an attempt to calculate cutting temperatures was made by Usui et al. [40], and by relying on a wear model developed by Trigger and Chao [41] a numerical simulation to predict crater wear in carbide tools was developed. Nonetheless, acquiring parameters for the aforementioned wear model depends on the accuracy of the temperature measurement obtained for the cutting process.

It is acknowledged that the wear model used in this study is oversimplified; however it still delivers a qualitative understanding of the temperature profiles within the vicinity of the contact zone. Moreover, it should be stressed that temperature values exceeding 1200 °C that were calculated using the current FE simulations are not supported by adequate material properties data, and thus, must be treated cautiously.

The EDX analysis of wear debris for low sliding velocity tests (1 – 7.5 m/s) indicates less wear on the ceramic side in comparison to the metallic counterface. This is confirmed by the concentration of elements originating from the ceramic in comparison to those originating from Inconel 718, Fig. 13.

At higher sliding velocities, the highest concentrations appear to be for Si, O, and N indicating a higher proportion of the wear debris to come from the ceramic. By considering the contact surface temperature difference obtained from the FE simulations for the ceramic sample and Inconel 718 disk, Fig. 16, it appears that the heat generated at high sliding velocities causes a steep rise in the temperature of the ceramic tip and thus, results in a substantial loss of strength and hardness of silicon nitride (the room-temperature four-point bending strength of SN-GP black is 679.9 MPa, which drops to 493.4 MPa at 1000 °C [19]). On the other hand, while not being in continuous contact at the same location, the metallic disk is able to dissipate the heat and remain at much lower temperatures and therefore, retains its strength. Hence, it can be concluded that at high sliding velocities (and analogously high cutting speeds) the wear rates of silicon nitride may be too high for application in cutting nickel-base alloys and therefore, an optimum range of working conditions has to be identified to be able to achieve low friction and low wear rates in the ceramic tool.

6 Conclusions

Dry sliding experiments on silicon nitride against Inconel 718 were conducted in conjunction with finite element simulations of contact with an implemented wear model. The results can be summarized as follows:

The COF decreases with increasing sliding velocity and shows a minimum at the highest sliding velocity. The same behavior was observed when the COF is plotted against the frictional power.

Wear rates (or wear coefficients) show a decrease with increasing sliding velocities and reach a minimum, beyond which wear increases with increasing sliding velocity. The same behavior was observed for wear as a function of frictional power. It was shown that despite the considerable drop in contact pressure due to geometrical changes, wear rates at high sliding velocities were mostly related to the high contact surface temperatures.

The dominant wear mechanism in dry sliding of silicon nitride against Inconel 718 is directly related to the sliding velocity. Moreover, it can be correlated with localized contact surface conditions, and in particular the surface contact temperature and contact pressure. At low sliding velocities,

mechanically induced wear (attrition and fatigue) is dominant in the ceramic. It is characterized by high COF and rather moderate wear rates. Increasing the sliding velocity and the consequent increase in contact surface temperatures gradually masks mechanically induced wear in favor of tribochemical wear. This phase is characterized by moderate COF and lowest wear rates. Extreme contact surface temperatures induced by high sliding velocities trigger faster chemical reactions and thus, lead to dominant tribochemical wear in the ceramic characterized by low COF and high wear rates. At such temperatures, the ceramic undergoes a considerable loss of strength and hardness resulting in an inefficient cutting process.

7 Acknowledgements

The research leading to these results has received funding from the European Union's Seventh Framework Program FP7/2007-2013 under grant agreement no. 263476.

8 References

[1] G. Stachowiak and G. Stachowiak, "Wear behaviour of ceramic cutting-tools," *Key Engineering Materials,* vol. 96, pp. 137-164, 1994.

[2] B. Kramer, "On tool materials for high speed machining," *Journal of Engineering for Industry,* vol. 109, no. 2, pp. 87-91, 1987.

[3] J. Olortegui-Yume and P. Kwon, "Tool wear mechanisms in machining," *International Journal of Machining and Machinability of Materials,* vol. 2, no. 3/4, pp. 316-334, 2007.

[4] D. Zhu, X. Zhang and H. Ding, "Tool wear characteristics in machining of nickel-based superalloys," *International Journal of Machine Tools and Manufacture,* vol. 64, pp. 60-77, 2013.

[5] S. Pervaiz, A. Rashid, I. Deiab and M. Nicolescu, "Influence of tool materials on machinability of titanium- and nickel-based alloys: A review," *Materials and Manufacturing Processes,* vol. 29, p. 219–252, 2014.

[6] S.-T. Buljan and S. Wayne, "Wear and design of ceramic cutting tool materials," *Wear,* vol. 133, no. 2, pp. 309-321, 1989.

[7] J. Vleugels and O. van der Biest, "Chemical wear mechanisms of innovative ceramic cutting tools in the machining of steel," *Wear,* vol. 225–229, p. 285–294, 1999.

[8] I. Khader, A. Renz, A. Kailer and D. Haas, "Thermal and corrosion properties of silicon nitride for copper die casting components," *Journal of the European Ceramic Society,* vol. 33, p. 593–602,

2013.

[9] J. Yeomans and T. Page, "The chemical stability of ceramic cutting tool materials exposed to liquid metals," *Wear,* vol. 131, no. 1, pp. 163-175, 1989.

[10] R. Silva, J. Gomes, A. Miranda and J. Vieira, "Resistance of Si3N4 ceramic tools to thermal and mechanical loading in cutting of iron alloys," *Wear,* vol. 148, no. 1, pp. 69-89, 1991.

[11] B. Mills, "Recent developments in cutting tool materials," *Journal of Materials Processing Technology,* vol. 56, no. 1-4, pp. 16-23, 1996.

[12] S. Casto, E. Valvo and V. Ruisi, "Wear mechanism of ceramic tools," *Wear,* vol. 160, no. 2, pp. 227-235, 1993.

[13] E. Ezugwu, J. Bonney, R. da Silva and A. Machado, "Evaluation of the performance of different nano-ceramic tool grades when machining nickel-base, Inconel718, alloy," *Journal of the Brazilian Society of Mechanical Sciences and Engineering,* vol. 26, no. 1, pp. 12-16, 2004.

[14] H. Addhoum and D. Broussaud, "Interaction of ceramic cutting tools with nickel-based alloys," *Materials Science and Engineering: A,* vol. 109, pp. 379-387, 1989.

[15] E. Trent and P. Wright, Metal Cutting, Woburn, MA: Butterworth-Heinemann, 2000.

[16] A. Renz, Untersuchung des Verschleißverhaltens von keramischen Schneidstoffen im trockenen Gleitreibungskontakt mit Nickelbasislegierungen, PhD Thesis, Stuttgart: Fraunhofer Verlag, 2015.

[17] S. Bhattacharyya, A. Jawaid, M. Lewis and J. Wallbank, "Wear mechanisms of Syalon ceramic tools when machining nickel-based materials," *Metals Technology,* vol. 10, no. 1, pp. 482-489, 1983.

[18] A. Renz, I. Khader and A. Kailer, "Tribochemical wear of cutting-tool ceramics in sliding contact against nickel-base alloy"," *Journal of the European Ceramic Society,* no. 36, pp. 705-717, 2016.

[19] *EU-FP7-NMP, Enhanced reliability and lifetime of ceramic components through multi-scale modelling of degradation and damage RoliCer, ID: 263476,* 2011-2014.

[20] "INCONEL® Alloy 718," Special Metals Corporation, Sept. 2007. [Online]. Available: www.specialmetals.com.

[21] J. Barber, "Distribution of heat between sliding surfaces," *Journal of Mechanical Engineering Science,* vol. 9, p. 351–354, 1967.

[22] R. Komanduri and Z. Hou, "Analysis of heat partition and temperature distribution in sliding systems," *Wear,* vol. 251, p. 925–938, 2001.

[23] T. Quinn, "Oxidational Wear," in *ASM Handbook, Volume 18 - Friction, Lubrication, and Wear Technology*, P. Blau, Ed., ASM International, 1992, pp. 280-289.

[24] G. Fleischer, "Energetische Methode zur Bestimmung des Verschleißes," *Schmierungstechnik,* vol. 4, no. 9, pp. 269-274, 1973.

[25] G. Fleischer, "Zum energetischen Niveau von Reibpaarungen," *Schmierungstechnik,* vol. 16, no. 12, pp. 358-363, 1985.

[26] D. Shakhvorostov, K. Pöhlmann and M. Scherge, "An energetic approach to friction, wear and temperature," *Wear,* vol. 257, no. 1-2, pp. 124-130, 2004.

[27] I. Tomaszkiewicz, "Thermodynamics of silicon nitride standard molar enthalpy of formation of amorphous Si3N4 at 298.15 K," *Journal of Thermal Analysis and Calorimetry,* vol. 65, pp. 425-433, 2001.

[28] M. Yovanovich, "Recent developments in thermal contact, gap and joint conductance theories and experiment," in *Proceedings of the Eighth International Conference*, San Francisco, CA, 1986.

[29] N. Ravindra, S. Abedrabbo, W. Chen, F. Tong, A. Nanda and A. Speranza, "Temperature-dependent emissivity of silicon-related materials and structures," *IEEE Transactions on Semiconductor Manufacturing,* vol. 11, no. 1, pp. 30-39, 1998.

[30] "Table of Total Emissivity," OMEGA Engineering inc., 2003-2015. [Online].

[31] G. Greenea, C. Finfrock and T. Irvine Jr., "Total hemispherical emissivity of oxidized Inconel 718 in the temperature range 300–1000°C," *Experimental Thermal and Fluid Science,* vol. 22, no. 3-4, pp. 145-153, 2000.

[32] "Abaqus Analysis User's Manual, Version 6.14," Dassault Systèmes Simulia Corp., Providence, RI, 2014.

[33] R. Holm, Electric Contacts, Stockholm: Almquist and Wiksells Akademiska Handböcker, 1946.

[34] J. Archard, "Contact and rubbing of flat surfaces," *Journal of Applied Physics,* vol. 24, pp. 981-988, 1953.

[35] T. Jacobs, B. Gotsmann, M. Lantz and R. Carpick, "On the application of transition state theory to atomic-scale wear," *Tribology Letters,* vol. 39, no. 3, pp. 257-271, 2010.

[36] T. Jacobs and R. Carpick, "Nanoscale wear as a stress-assisted chemical reaction," *Nature Nanotechnology,* vol. 8, no. 2, p. 108–112, 2013.

[37] N. Gosvami, J. Bares, F. Mangolini, A. Konicek, D. Yablon and R. Carpick, "Mechanisms of antiwear tribofilm growth revealed in situ by single-asperity sliding contacts," *Science,* vol. 348, no. 6230, pp. 102-106, 2015.

[38] G. Brandt, A. Gerendas and M. Mikus, "Wear mechanisms of ceramic cutting tools when machining ferrous and non-ferrous alloys," *Journal of the European Ceramic Society,* vol. 6, no. 5, pp. 273-290, 1990.

[39] N. Narutaki, Y. Yamane, K. Hayashi, T. Kitagawa and K. Uehara, "High-speed machining of Inconel 718 with ceramic tools," *CIRP Annals - Manufacturing Technology,* vol. 42, no. 1, pp. 103-106, 1993.

[40] E. Usui, T. Shirakashi and T. Kitagawa, "Analytical prediction of three dimensional cutting process - Part 3 Cutting temperature and crater wear," *Transactions of the ASME,* vol. 100, pp. 236-243, 1978.

[41] K. Trigger and B. Chao, "The mechanism of crater wear of cemented carbide tools," *Transactions of the American Society of Mechanical Engineers,* vol. 78, pp. 1119-1126, 1956.